Radius measurement by interferometry

Lars A. Selberg
Zygo Corporation
Laurel Brook Road
Middlefield, Connecticut 06455

Abstract. The radius of curvature is a fundamental parameter of optical surfaces. Improving the measurement tolerance is critical for an increasing number of applications. Interferometry is potentially a very accurate technique, but careful implementation is critical to achieving full potential. To this end, the error budget for radius of curvature measurement by interferometry is examined. The goal is to achieve 0.001% (10 ppm) measurement tolerance. The major errors, Abbé errors, are typically 10 to 100 μm, and can be virtually eliminated using a distance-measuring interferometer. The remaining major errors are cavity null errors and axial alignment errors. These are quantified and corrections are described. Other errors including environmental and tooling errors are also cataloged.

Subject terms: interferometry; radius (of curvature).

Optical Engineering 31(9), 1961-1966 (September 1992).

1 Introduction

Radius of curvature measurement by interferometry is not a new technique.[1] Many optical shops use an interferometer and slide mechanism for accurate, noncontact radius measurement. Interferometry easily provides measurement of the radius of curvature to accuracies of 0.01%. In fact, with appropriate implementation, this accuracy can be pushed down into the range of 0.001% (10 ppm) and below. This level of measurement requires careful consideration of the measurement error budget, and it is the thrust of this paper to examine the control and correction of nonenvironmental, optical and optomechanical errors. After examining these errors, they are placed in the context of a summary error budget. Radius measurement is also very sensitive to site implementation and technique. Careful measurement procedure, control of environmental factors, and proper tooling design are essential to achieving the accuracy of which this measurement technique is capable.

The radius of a sphere is simply the distance from the spherical surface, or its best fit equivalent, to the corresponding center of curvature. These two locations are easily observed with a point source interferometer producing a converging wavefront, such as a Fizeau or Twyman-Green (see Fig. 1). At the "cat's-eye" position, the interferometer beam converges to a point on the spherical surface, the cat's-eye point. A nulled fringe pattern indicates the point focus is at the surface of the sphere. At the "confocal" position, a nulled fringe pattern indicates the interferometer point focus is coincident with the surface center of curvature. By measuring the distance that the part is moved between these null positions, i.e., from cat's-eye to confocal, the radius of curvature is determined.[1] This distance is most accurately measured if the measurement axis intersects both the cat's-eye point and the surface center of curvature, which will be called the part axis. Glass or magnetic scales can resolve motion at the micrometer level, but are displaced from the part axis, thereby incurring Abbé errors; for a displacement of 100 mm, Abbé errors of 10 to 100 μm are typical (see Fig. 2). Configurations with two scales on opposite sides of the part axis can reduce Abbé errors. To use only one measurement axis without suffering these errors, the measurement axis must be made coincident with the part axis by using a distance-measuring interferometer[1] (DMI). This reveals other error sources previously overshadowed. The following sections concentrate on two optical alignment errors: cavity null and axial alignment. The cavity null error is the error in finding the null position. The null error is evident in the fringe pattern; accurate evaluation and correction requires measurement of the cavity function via phase-measuring interferometry (PMI). Axial alignment errors arise from the part being translated along one axis and the motion being measured along another. This leads to cosine errors. Part of this error is visible in the interference pattern, and the alignment can be corrected. These errors are fundamental to the technique. Other errors, including environmental and tooling errors, are cataloged and briefly quantified.[2]

2 Equipment

The radius measurement equipment consists of a phase-measuring point source interferometer (e.g., Fizeau) with a transmission sphere (TS) or diverger lens, a DMI configured as a linear interferometer, and a rail/guide assembly with a mount with five axes of motion to hold the surface under test (see Fig. 3). The mount is moved along a rail/guide. This can be as simple as a precision ground straight-edge, against which a mount is located and moved. A virtue of the DMI is that the rail specifications are greatly relaxed.

The moving corner cube of the linear interferometer (DMI) is affixed to the part mount so that its apex is on the part axis. There are two possible implementations: z tracking—

Paper 05012 received Jan. 14, 1991; revised manuscript received April 6, 1992; accepted for publication April 6, 1992.

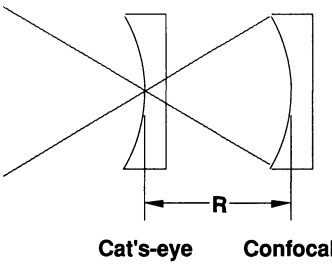

Fig. 1 Radius measurement geometry, showing cat's-eye and confocal measurement positions.

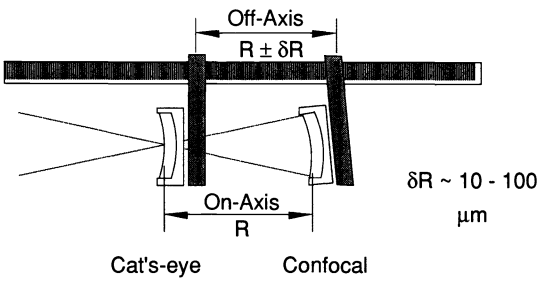

Fig. 2 Abbé errors are caused by measuring along an axis displaced from the axis of motion.

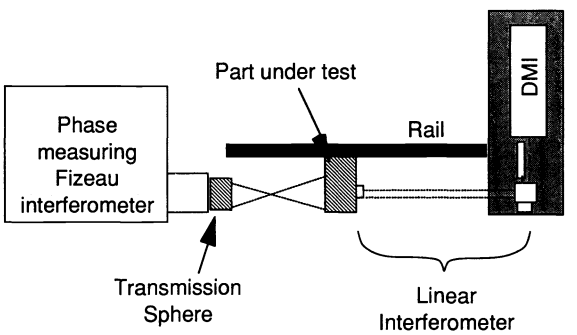

Fig. 3 Interferometric radius measurement system including phase-measuring Fizeau interferometer with transmission sphere, DMI with linear interferometer, five-axes mount, and guide.

in which the moving cube is mounted only to the z adjustment (focus) of the mount and therefore cannot monitor either lateral direction or the tip/tilt functions—and fully tracking—in which the moving cube is mounted at the part and therefore can follow any lateral or tip/tilt motion of the part, which is along the DMI axis. The z tracking implementation has the advantage that the DMI signal cannot be lost during lateral motion of the part.

3 Error Sources

3.1 *Null Cavity Errors*

The position error caused by a nonnulled cavity is derived from the sag equation for a sphere.[2,3]

$$\delta R_{\text{null}} = \frac{\varphi\lambda}{1-[1-1/(2F_{\text{limit}})^2]^{1/2}} , \qquad (1)$$

where φ is the focus error in waves, i.e., the sag at the edge of the aperture; F_{limit} is the limiting F number of the interferogram at a given position; and λ is the operating wavelength of the interferometer, typically 633 nm. At cat's-eye, $F_{\text{limit}} = F_{\text{TS}}$, the F number of the transmission sphere, while at confocal the limiting aperture is usually the R number of the surface under test. The error is an absolute error and is large for large F number (see Fig. 4). PMI enables correction of the null error by measuring the power in the interference pattern. Equation (1) is then used to correct the longitudinal error. There are some second-order errors in this correction, which can be quantified and reduced through careful technique.

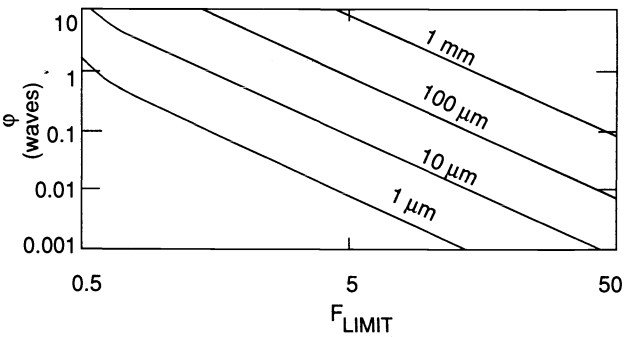

Fig 4 Cavity power φ versus limiting F number, F_{limit} for four values of cavity null error δR. A typical value for nulling the cavity by eye, with tilt fringes, is 0.1 waves. Without tilt, 0.25 waves is more typical.

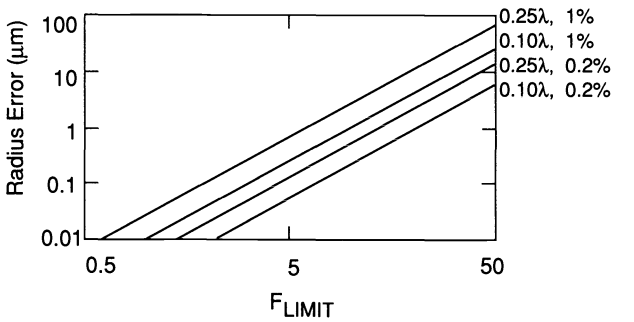

Fig 5 Fractional error in the null correction term due to F number calibration accuracy of 1% and 0.2%, for 0.1 λ and 0.5λ of residual power in the interference pattern.

At both positions of the phase measurement, the limiting aperture must be known for Eq. (1). If there is an error in the actual F number, an error results in the null correction term. This error is absolute in terms of the radius of curvature and relative to the null correction term. Thus, F number calibration errors are smaller for fast, well-nulled cavities (see Fig. 5). The R number of the surface is usually easy to determine. Except for very small parts, the diameter of the spherical surface can be measured to within 1% accuracy quite easily. The F number of a transmission sphere/diverger lens, and its uncertainty can be determined by ray-tracing the design (see Appendix B).

Distortion of the image causes an error in the calculation of the power in the cavity. Rewriting Eq. (1), the mapping of the cavity phase is given by

$$\varphi = \frac{\delta R}{\lambda}(1-\cos\theta) . \qquad (2)$$

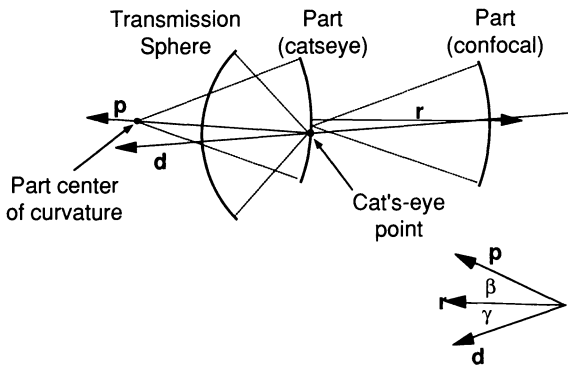

Fig. 6 Relevant axes for radius measurement, **p**, **r**, and **d**.

This is mapped into the image space via $r = f(\theta)$, and then fit to

$$\varphi = cr^2 + \text{lower-order terms} \ . \tag{3}$$

Typically, the error in the calculated cavity power is $< 1\%$ for a fast TS and approaching ppm levels for a slow TS (see Appendix B). This should not be confused with the peak-to-valley (PV) errors caused by distortion, which can be as large as 10% of the power for a fast TS. Such small errors in power are of little consequence because of the form of Eq. (1). Thus, aperture calibration is a more significant error than distortion. In both cases, the error is a fraction of the null error term, and therefore care in nulling the cavity is recommended.

3.2 *Axial Alignment Errors*

There are three axes that are important for radius measurement, **d** (DMI beam), **r** (axis of motion), and **p** (part axis). The angles between these are $\alpha(\mathbf{p},\mathbf{d})$, $\beta(\mathbf{p},\mathbf{r})$ and $\gamma(\mathbf{r},\mathbf{d})$ (see Fig. 6). The net motion of the part along the part axis is R, the surface radius. The axial error is a relative error. For the fully tracking configuration, the error depends solely on the alignment of the part axis to the DMI:

$$\delta R_{\text{axial}} = R(1 - \cos\alpha) \ . \tag{4}$$

For the z-tracking configuration, the error is compound, depending on the part alignment β and the system alignment γ:

$$\delta R_{\text{axial}} = R(1 - \cos\beta \cos\gamma) \ . \tag{5}$$

To achieve an accurate measurement, the net motion of the surface between the cat's-eye and confocal positions must be in the direction of the part axis and the DMI must measure all motion in this same direction, i.e., the **p**, **r**, and **d** axes must be parallel. The alignment of the interferometer axis and the TS relative to the other axes have no detrimental effect on the DMI measurement accuracy; misalignment will place the surface off-center at the confocal position, limiting the F number that can be measured. It is assumed that the angle errors do not change during the measurement process. The z-tracking configuration is assumed throughout the rest of this paper.

Part alignment is a two step process ensuring that (1) the cat's-eye reflection is not sheared with respect to the incident beam, i.e., no vignetting, and (2) when moved to confocal, tilt is minimized without additional tip/tilt or lateral adjustments. Part misalignment β can be measured:

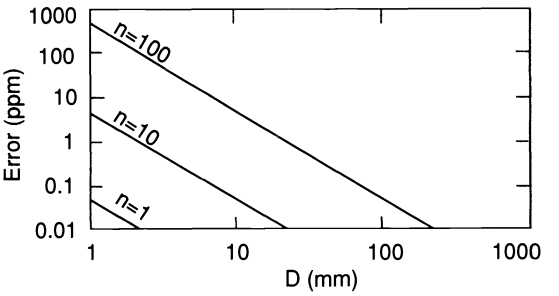

Fig. 7 Radius measurement error due to axial alignment error of part to rail β as a function of part diameter D (scaled from 1 μm to 1 m), for $n = 1$, 10, and 100 tilt fringes visible at confocal; $\gamma = 0$.

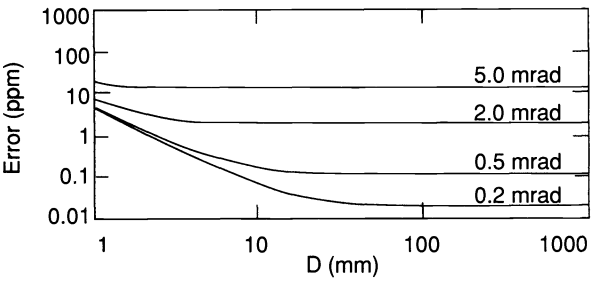

Fig. 8 Radius measurement error for $n = 10$ fringes and $\gamma = 0.2$, 0.5, 2, and 5 mrad, as a function of part diameter.

$$\tan\beta = \frac{n\lambda}{2R} F_{\text{limit}} \ , \tag{6}$$

where $n\lambda$ is the tilt at confocal and R is the test surface radius of curvature. Careful alignment technique must be used to avoid large numbers of tilt fringes being introduced. Only when a large number of fringes, > 10, are introduced and the part diameter is small, < 10 mm, is the error significant to the measurement. If 10 ppm measurement accuracy is to be achieved over the entire range of expected part diameters and radii, special attention must be paid to the alignment of small diameter parts. The cosine error due to the angle β can be corrected by measuring the tilt at the confocal position and dividing by $\cos(n\lambda/2D)$. Figure 7 shows that this error is rarely significant, except for very small diameter parts.

Misalignment of the rail and DMI γ has the effect of adding a nonzero baseline to the axial error (see Fig. 8). One can measure γ by observing the runout of the return spot of the DMI as the part mount is moved:

$$\tan\gamma = \frac{\text{return spot runout}}{2 \cdot \text{total motion of mount}} \ . \tag{7}$$

Note that $\gamma = 0.5$ mrad is easily achieved if the mount has a full travel range of 1 m.

3.3 *Figure Error*

In general, the cat's-eye point does not lie on the best fit sphere to the surface, i.e., it has some height relative to the best fit sphere. This is the figure error. It is a small error,

Table 1 Approximate ranking of error sources for some ranges of part radii of curvature and *R* number. Errors are grouped as catastrophic, significant, and negligible, relative to a net error budget of 10 ppm (0.001%). Assumptions regarding certain parameters of measurement are outlined in the footnote.

	Radius of Curvature			
	10 mm	**100 mm**	**1 m**	**10 m**
R/0.5	Abbé Shop Tooling Null Lab Corrected null Figure Air index Align "short" Align "typical" Corrected index	Abbé Shop Tooling Null Air index Lab Corrected null Figure Align "typical" Corrected index	Abbé Air index Shop Tooling Null Lab Align "typical" Air index Corrected null Figure Align "long"	Abbé Air index Shop Tooling Corrected index Null Lab Corrected null Figure Align "long"
R/2	Abbé Null Shop Tooling Corrected null Lab Figure Air index Align "short" Align "typical" Corrected index	Abbé Null Shop Tooling Air index Corrected null Lab Align "short" Figure Align "typical" Corrected index	Abbé Null Air index Shop Tooling Corrected null Lab Align "typical" Corrected index Figure Align "long"	Abbé Air index Null Shop Tooling Corrected index Corrected null Lab Figure Align "long"
R/10	Null Abbé Corrected null Shop Tooling Lab Figure Align "typical" Air index Align "short" Corrected index	Null Abbé Corrected null Shop Tooling Air index Lab Figure Align "long" Align "typical" Corrected index	Null Abbé Corrected null Air index Shop Tooling Lab Align "typical" Corrected index Figure Align "long"	Null Abbé Air index Corrected null Shop Tooling Corrected index Lab Figure Align "long"
R/50	Null Corrected null Abbé Shop Tooling Align "typical" Lab Figure Air index Align "short" Corrected index	Null Corrected null Abbé Shop Tooling Align "long" Air index Lab Align "typical" Figure Corrected index	Null Corrected null Abbé Air index Shop Tooling Lab Align "typical" Corrected index Figure Align "long"	Null Corrected null Abbé Air index Shop Tooling Corrected index Lab Figure Align "long"

Abbé	Abbé errors due to off-axis measurement 50 μm
Null	0.5 fringes
Corrected null	residual error due to 1% aperture calibration error and distortion
Air index	5 ppm (5°C deviation from STP)
Corrected index	0.12 ppm (Edlen's equation)
Alignment errors:	"typical" 10 fringes tilt $\gamma = 0.5$ mrad
	"long" 20 fringes tilt $\gamma = 0.1$ mrad
	"short" 1 fringe tilt $\gamma = 2.0$ mrad
Figure	0.1λ of SA3
Shop	Air turbulence and vibration present in typical shop environment
Lab	Air turbulence and vibration present in well designed metrology lab
Tooling	Errors due to tooling sag and thermal gradients for "typical" conditions

always less than the peak-to-valley (PV) surface error. As an example, if the surface is dominated by third-order spherical aberration, the PV error relative to the best fit sphere and the figure error are

$$PV_{SA3} = \frac{SA3}{4} , \tag{8}$$

$$\delta R_{figure} = \frac{SA3}{6} = \frac{2}{3} PV_{SA3} , \tag{9}$$

where SA3 is the wave aberration coefficient for third-order spherical aberration. In general, the figure of the surface is irregular. Figure error can be calculated from the PMI data and corrected. The accuracy of the correction depends on the accuracy to which the cat's-eye point can be identified. Correction to within 10% of δR_{figure} is readily achievable with smooth surfaces.

3.4 *Error Summary*

Cavity null, axial alignment errors and figure errors are by no means the only ones present in measurements. There are other optical errors as well as environmental and tooling errors and noise; more thorough discussion of these errors can be found elsewhere.[2] All error contributions are summarized in Table 1. For each radius of curvature and R number combination in the table, the error sources are listed in order of severity. They are grouped in the categories of catastrophic, significant, and negligible, relative to a net error budget of 10 ppm. Various assumptions about the test technique and facility are made, and therefore, Table 1 is a rule of thumb only. Actual error contributions depend on the technique of the metrologist and the design of the tooling and facility.

Observing the trends of Table 1, it is possible to conclude several points:

- Without on-axis measurement (use of a DMI), radius of curvature measurement to 10 ppm is not feasible due to Abbé errors.
- Extreme care of nulling the cavity and accurate calibration of the apertures is essential to achieving 10-ppm accuracy for a very short radius of curvature ($\sim$ 10 mm) or very slow ($\sim R/50$) parts.
- Wavelength compensation[4] for the DMI, or accurate atmospheric control, is essential for 10-ppm testing at all but the shortest radii.
- If reasonable care is taken in aligning the DMI, rail, and part axes, these errors are kept negligible, except in the case of very short radius parts.

Among other "negligible" errors not listed in Table 1 are various noise sources, mostly from the DMI: linearity, resolution, polarization mixing, thermal effects, laser wavelength stability, power calculation accuracy, etc. These errors are typically so small that they will always be an order of magnitude smaller than the other errors discussed here.

4 Conclusions

The accuracy of radius measurement by interferometry is greatly enhanced when a DMI is used to measure the motion of the surface under test along the part axis. Further correction of the null cavity errors and wavelength compensation can limit the remaining errors to the micrometer level, or less. The bulk of these errors must be corrected through design of the tooling and the metrology facility. Testing at the level of 0.001% (10 ppm) is feasible for parts with radius $>$ 100 mm. For shorter radii, turbulence and tooling errors become severe, typically limiting measurement accuracy to the micrometer range.

Table 2 Parameters defining the part under test, the measurement system, and the environmental parameters for the error budget shown in Table 3.

Part	Radius of Curvature	200 mm
	R/number	5 ±1%
	Figure	λ/10 PV (SA3)
Interferometers	Figure measurement	Zygo MARK IV*xp* with f/3.3 TS
	DMI	Zygo Axiom 2/20
Alignment	Null at cat's-eye	0.5 fringe
	Null at confocal	0.2 fringe
	Part axis (β)	10 tilt fringes at confocal
	DMI axis (γ)	0.5 mrad
Atmospheric	Offset from STP	5 °C, 30 mm Hg, 30% RH
	Drift during measurement	0.1 °C, 1 Torr, 2% RH
Tooling	Longitudinal sag	1 micron
	Decenter during measurement	25 microns
	Longitudinal separation of corner cube and cat's-eye point	100 mm
DMI errors	as per Zygo Axiom 2/20 with linear interferometer	0.01 μm
	interferometer dead-path	500 mm
Vibration	as observed in a "typical" shop environment with	4.12 μm in shop, 0.40 μm in lab
Air Turbulence	an air isolated table and in a metrology lab environment	

Table 3 A summary error budget for radius-of-curvature measurement. Abbé errors are not included in this budget. Typical Abbé errors can be in the range of 10 to 100 μm, greatly exceeding the other errors.

Error type			uncorrected	corrected	residual after correction
Optical	Null	confocal	12.62	0.64	Aperture calibration and distortion
		cat's-eye	13.94	0.11	
	Figure	SA3	0.07	0.01	~10% of PV
Axial Alignment	All		0.14	0.14	γ error
Environment	Atmospheric, Vibration		5.28	0.52	air turbulence and vibration, 0.12 ppm from air index of refraction
Tooling			1.25	0.35	Facility and tooling design
DMI/computational			0.02	0.02	Fixed errors
Total			33.31	1.78	microns
			167	8.9	ppm

Table 4 Nominal and actual F numbers of the more common Zygo 4-in. transmission spheres as well as the aperture uncertainty and distortion coefficient.

Nominal	Design	Worst case deviation from design	Distortion coefficient
0.65	0.638	0.2%	0.96%
0.75	0.738	0.2%	0.42%
1.5	1.502	0.4%	0.02%
3.3	3.328	0.4%	<1ppm
7.2	7.105	0.4%	<1ppm
11	11.000	<0.01%	<1ppm

5 Appendix A: Sample Error Budget

A sample error budget is shown here for interferometric radius of curvature measurement. The system parameters are given in Table 2, and the error budget is shown in Table 3. Environmental and tooling error contributions have been chosen to reflect a well-designed facility.[2]

6 Appendix B: Zygo Transmission Sphere Parameters

Table 4 shows the aperture and distortion characteristics for some of the Zygo transmission spheres.

Acknowledgments

Thanks are due to George Hunter who initiated null error correction and provided insight in other areas, to Peter Pfluke

who wrote a radius measurement package with null error correction and did much testing of system accuracy and repeatability, and to Mike Stielau who provided several of the figures.

References

1. J. Bruning, "Fringe Scanning Interferometers," in *Optical Shop Testing*, D. Malacara, Ed., John Wiley & Sons, Inc., p. 428 (1978).
2. L. A. Selberg, "Zygo interferometric radius scale system description and analysis," Zygo Application Bulletin AB-0050, Zygo Corporation, (1990).
3. W. J. Smith, *Modern Optical Engineering*, McGraw-Hill, New York (1966).
4. W. Tyler Estler, "High accuracy displacement interferometry in air," *Appl. Opt.* **24**(6), 808–815 (1985).

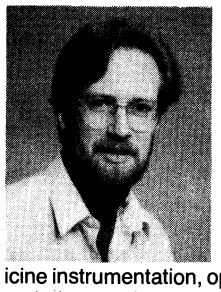

Lars A. Selberg is a senior optical engineer at Zygo Corporation, where his work encompasses instrument design, applications development, and customer support. He has presented papers on interferometer accuracy and other interferometric measurement techniques and holds an MS in optical sciences from the University of Arizona and an SB in physics from the Massachusetts Institute of Technology. His prior work has been in the fields of nuclear medicine instrumentation, optical scattering diagnostics, x-ray astronomy, and plasma physics.